Apolipoprotein C-II induces EMT to Promote Gastric Cancer Peritoneal Metastasis via PI3K/AKT/mTOR Pathway

Chao Wang
Nanjing University
Zhi Yang
Nanjing Medical University
En Xu
Nanjing University
Xingzhou Wang
Nanjing University
Zijian Li
Nanjing Medical University
Heng Yu
Nanjing Medical University
Kai Chen
Nanjing University
Song Liu
Nanjing University
Wenxian Guan (guan_wenxian@sina.com)
Nanjing University https://orcid.org/0000-0002-2171-6265

Research

Keywords: Peritoneal metastasis, APOC2, EMT, PI3K/AKT/mTOR, Invasion

Posted Date: February 12th, 2021

DOI: https://doi.org/10.21203/rs.3.rs-204281/v1

Abstract

Background: Peritoneal metastasis (PM) occurs frequently in patients with gastric cancer (GC) and confers poor survival. Lipid metabolism and epithelial-mesenchymal transition (EMT) play an important role in GC metastasis. As Apolipoprotein C-II (APOC2) is a key protein in lipid metabolism, few studies have investigated the role of APOC2 in PM. This study aims to elucidate the potential molecular mechanism of APOC2 in the PM of GC.

Methods: The Tandem Mass Tagging (TMT) method followed by liquid chromatography-tandem mass spectrometry-based proteomics analysis was used to compare the levels of differentially expressed proteins between human PM and GC tissues. APOC2 expression was evaluated by immunoblotting, and immunohistochemistry analysis (n = 111). *APOC2* over-expression and knock-down expression cell models were developed and tested in vitro. RNA sequencing analysis evaluated the changes in gene expression after *APOC2* knockdown in GC cells. The Agilent Seahorse XF platform and lipid staining assay were used to evaluate the role of APOC2 in lipid metabolism of GC cells. Spheroid cell invasion assay, apoptosis assay, colony formation assay, wound-healing assays, and transwell assays were performed and peritoneal implants into nude mice were done to assess the biological effects of APOC2. The underlying mechanisms were investigated using Western blot, inhibitor or activator treatment assays.

Results: APOC2 was highly abundant in GC cells and PM tissues. And high APOC2 levels in GC tissues correlated with poor patient prognosis. Knockdown of *APOC2* inhibited the malignant phenotype of cancer cells and EMT significantly. Massive gene expression alterations after APOC2 knockdown, which were associated with various signaling pathways, especially the PI3K/AKT signaling pathway and lipid metabolism. Furthermore, the regulatory effects of APOC2 on the EMT were partially attributed to the PI3K/AKT/mTOR signaling pathway. The results in vivo also showed that APOC2 modulated GC PM.

Conclusions: We verified that knockdown of *APOC2* suppressed GC cell Lipid metabolism, proliferation, migration, invasion, and EMT, accompanied by inactivation of PI3K/AKT/mTOR signaling pathway. *APOC2* overexpression had the opposite effects GC cell phenotypes and mechanisms. Collectively, our results identified APOC2 in PM as a potential therapeutic target.

Background

Gastric cancer (GC) is a major health problem worldwide, especially in China. It ranks third in cancer related deaths worldwide and is associated with huge health costs and patient pain, especially in eastern Asia, mainly because of the high incidence of recurrence and metastasis (1, 2). Peritoneal metastasis (PM) is a frequent pattern of metastasis in patients with advanced GC (3). PM represents a major challenge to patients and clinicians (4–6).The quality of life of patients with PM is poor and their survival is short (7). The molecular mechanisms underlying PM are poorly understood. Thus, in-depth mechanistic research is required to discover the driving factors of PM and develop an effective treatment.

Apolipoprotein C-II (APOC2) binds to triglyceride-rich lipoproteins (TRL), such as chylomicrons (CM) and very low-density lipoproteins (VLDL), and high-density lipoproteins (HDLs) (8, 9). The human *APOC2* gene is located in the human *APOE-APOC1-APOC4-APOC2* gene cluster on chromosome 19 and its transcriptional control is complex (10, 11). APOC2 is synthesized mainly by the liver and is then secreted into the plasma to bind lipids and lipoprotein lipase (LPL); however, it is also expressed in other tissues, including macrophages and the intestine, where it regulates lipolysis at the local level (12–14). APOC2 plays an important role in TRL metabolism because it can guide lipoproteins to active LPL sites and act as a physiological activator of LPL, which is the main enzyme that hydrolyzes plasma triglycerides (TG) on TRLs (15–17). Therefore, APOC2 can provide energy transport and storage for cells by regulating lipid metabolism (18). APOC2 deficiency can cause severe hypertriglyceridemia and lead to cardiovascular disease (19, 20). However, reports on the role of APOC2 in cancer are scarce.

In epithelial-mesenchymal transition (EMT), immobile epithelial cells lose their cell identity and acquire an active mesenchymal phenotype, which has been recognized as a key factor in the invasion and metastasis of malignant tumors, including GC (21, 22). During EMT, GC cells lose their apical-basal polarity and acquire a mesenchymal phenotype, accompanied by the loss of E-cadherin expression in epithelial cells, and increased levels of mesenchymal markers, such as N-cadherin, Vimentin, Snail, Slug, Twist1, and matrix metalloproteinases (MMPs) (23, 24). Evidence indicates that phosphoinositide 3kinaseprotein kinase B-mammalian target or rapamycin (PI3K-AKT-mTOR) signaling is essential for EMT of malignant tumors (25). The continuous stimulation of PI3K-AKT and its downstream mTOR pathway targets leads to an aggressive cancer phenotype, including apoptosis resistance, invasion, and metastasis (26). However, how APOC2 regulates PI3K/AKT signaling and EMT in the progression of PM in GC is unknown. Therefore, it is urgent to explore the mechanism of APOC2 in EMT and PI3K/AKT/mTOR signal transduction to prevent PM of GC.

In the present study, we evaluated differences in the levels of proteins between primary GC tissues and corresponding PM tissues to identify differentially expressed proteins (DEPs) possibly involved in GC PM using tandem mass spectrometry-based proteomics and bioinformatic analyses. The results showed that APOC2 is a potential biomarker to detect PM in GCs. In addition, we compared the effect of *APOC2* knockdown in AGS cells with that in untreated AGS cells at the transcriptome level and identified differentially expressed genes (DEGs) that are involved mainly in lipid metabolism and tumor cell biological processes, including PI3K/AKT signaling. Combining the proteome and transcriptome data with the *in vitro* and *in vivo* experiments, we demonstrated that APOC2 can regulate GC EMT through the PI3K/AKT/mTOR signaling pathway to promote PM. To the best of our knowledge, this is the first study to combine GC cell transcriptomics and the proteomics of PC tissues from patients with GC.

Materials And Methods

Human tissue specimens of patients with GC

Surgical specimens of primary GC tissue and corresponding PM tissue used for mass spectrometry detection were obtained from five patients with GC (Nanjing Drum Tower Hospital, The affiliated Hospital of Nanjing University Medical School, Nanjing, China). This study enrolled 111 patients who were diagnosed with primary GC from January 2014 to December 2019 at Nanjing Drum Tower Hospital. According to the criteria of the American Joint Committee on Cancer, all these patients were diagnosed pathologically as having gastric adenocarcinoma. None of these patients received preoperative chemotherapy or radiotherapy. The GC tissues, the corresponding noncancerous mucosal tissues, and PM tissues were collected from all patients and washed with ice-cold phosphate-buffered saline (PBS) (GE Healthcare, Beijing, China) to remove residual blood after surgical resection and then immediately snap-frozen in liquid nitrogen and stored at − 80°C for further analyses. All patients provided written informed consent. This study was conducted according to the principles of the Declaration of Helsinki and was approved by the Hospital Ethics Committee of the Affiliated Drum Tower Hospital of Nanjing University Medical School.

Cell lines and culture

Human gastric adenocarcinoma cell lines, AGS, BGC-823, MGC-803, MKN-45, SNU-16, and GES-1 were purchased from Shanghai Cafa Biological Technology Co. Ltd. (Shanghai, China). The cells were cultured in Dulbecco's modified Eagle's medium (DMEM; Gibco, Waltham, MA, USA) supplemented with 10% fetal bovine serum (Gibco, Waltham, MA, USA) and 1% penicillin/streptomycin (Gibco).

Tandem Mass tag (TMT) Quantification Proteomic analysis

GC tissues and corresponding PM tissues were sampled from five patients with GC and combined. The samples were prepared and the differentially expressed proteins (DEPs) were determined using Liquid chromatography–tandem mass spectrometry (LC-MS/MS)-based proteomic and bioinformatic analyses at the Beijing Genomics Institution (BGI). For details, see Supplementary Materials and Methods.

Small interfering RNA (siRNA) design and transfection

To inhibit the expression of APOC2, gastric cells were transfected with APOC2-specific siRNAs (siRNA1, 5'-UCCUCCUGGUAUUGGGAUUTT-3',5'-AAUCCCAAUACCAGGAGGATT-3’; siRNA2, 5'-CCCAGAACCUGUACGAGAATT-3',5'-UUCUCGUACAGGUUCUGGGTT-3'; siRNA3, 5'-GCCAUGAGCACUUACACAGTT-3', 5'-CUGUGUAAGUGCUCAUGGCTT-3') or non-specific siRNA (10 μmol/L) synthesized by Shanghai GenePharma Company (Shanghai, China). Cells plated in six-well plates (200,000 cells/well) were transfected with siRNA duplexes (1–2 μg) encapsulated by the interferin reagent (Polyplus, New York, NY, USA), according to the manufacturer’s instructions. First, 6 pmol of siRNA were diluted in 200 μL of medium without serum, vortexed for 10 s, and pelleted by centrifugation. Then, 7 μL of interferin reagent was added, vortexed for 10 s, pelleted, and incubated for 10 min at room temperature (RT, 25°C). Finally, the transfection mixture was added to the cells in serum containing medium. The knockdown efficiency was tested using western blotting.

Lentivirus transductions

The lentiviral vector containing gene-specific short hairpin RNAs (shRNAs) against APOC2 and a control lentiviral vector encoding a scrambled shRNA were purchased from Shanghai Gene-Pharma Co., Ltd. To overexpress APOC2 in GC cells, lentiviral particles containing human full-length APOC2 were prepared by OBiO Technology Corp., Ltd (Shanghai, China) and used to infect GC cells. Human GC cell lines were transduced with the lentiviral particles along with polybrene and were selected using puromycin (1 mg/mL) (Thermo Fisher Scientific, Waltham, MA, USA) for 3 weeks.

Western blotting analysis

Total protein was extracted from tissues or cultured cell samples using Radioimmunoprecipitation assay (RIPA) lysis buffer containing protease inhibitor cocktail (Roche Applied Science, Penzberg, Germany) and centrifuged at 12000 × g at 4°C for 15 minutes. Supernatants were mixed with sodium dodecyl sulfate-polyacrylamide gel electrophoresis (SDS-PAGE) sample-loading buffer, boiled for 8 minutes, and then subjected to SDS-PAGE. After being transferred onto polyvinylidene fluoride membranes (Millipore, Billerica, MA, USA), non-specific binding was blocked using 5% nonfat milk. The blots were probed with the following primary antibodies follows: anti-APOC2, anti glyceraldehyde-3-phosphate dehydrogenase (GAPDH) (Abcam, Cambridge, MA, USA); anti-phospho (p)-PI3K, anti-AKT, anti-p-AKT, anti-MTOR, anti-p-mTOR, anti-E Cadherin, anti-N-Cadherin, anti-Vimentin, anti-snail, anti-slug, and anti-TWIST1 (Cell Signaling Technology, Danvers, MA, USA); anti-MMP9 and anti-MMP2 antibody (ProteinTech Group, Rosemont, IL, USA).

Immunohistochemical staining and scoring

The tissues were fixed in 10% formalin and then embedded in paraffin. The specific steps were performed as described previously. For each sample, the total score was based on the staining intensity and the ratio of positively stained tumor cells. The staining intensity was divided into 0 (no staining), 1 (light yellow), 2 (yellow brown), and 3 (brownish-yellow), and the ratio was graded as 0 (no positively stained cells), 1 (< 10%), 2 (10–50%), and 3 (> 50% of positive cells). The score was then calculated as staining intensity score multiplied by the ratio grade. A sample score of 0 to 2 was defined it as low expression, and 3 to 9 represented expression.

Reverse transcription quantitative real-time polymerase chain reaction (RT-qPCR) analysis

Total RNA was isolated from GC cells using Trizol reagent (Invitrogen, Carlsbad, CA, USA) according to the manufacturer's instructions, and then reverse-transcribed into cDNA using an RT-PCR kit (Takara, Kyoto, Japan). The RT-PCR assays were performed using SYBR Green Premix Ex Taq on an ABI ViiA 7DX RT-PCR machine (Applied Biosystems, Foster City, CA, USA). The relative gene expression was normalized to that of human GAPDH. Relative mRNA expression was calculated according to the 2-ΔΔCt method. The specific primer sets used for this assay included APOC2 (forward: TGTCCTCCTGGTATTGGGATTT, reverse: TGTCTTCTCGTACAGGTTCTGG), GAPDH (forward: GGAGTCCACTGGCGTCTTCA, reverse: GTCATGAGTCCTTCCACGATACC).

Seahorse and cellular metabolic analysis

The oxygen consumption rate (OCR) and extracellular acidification rate (ECAR) were determined in AGS and BGC823 cells using the Agilent Seahorse XF platform and Seahorse XF Real-Time ATP Rate Assay Kit (Agilent, Santa Clara, CA, USA). Briefly, 2000 *APOC2* knockdown cells and untreated cells were seeded in each well of Poly-D-Lysine (10 μg/mL, Sigma, St. Louis, MO, USA; P6407) coated 96-well Agilent Seahorse XF Cell Culture Microplate, separately. The plate was centrifuged at 200 · *g* without braking for 1 min. Oligomycin and Rotenone + antimycin A were dissolved and diluted in assay medium and loaded into the sensor cartridge at final concentrations of 1.5 and 0.5 μM, respectively.

Gene set Enrichment Analysis (GSEA)

All the gene sets were retrieved from mSigDB (https://www.gsea msigdb.org/gsea/index.jsp). The input data was pre-ranked using the log2-FoldChange. GSEA was carried out to explore the biological functions and pathways of genes. The R package “clusterProfiler 3.16.1” was used to perform the analysis and plot the results. The enrichment results that satisfied two conditions of p value < 0.05 and q value < 0.05, which indicated statistical significance.

RNA sequencing analysis

The mRNA of the AGS cells knocked down for APOC2 expression and untreated AGS cells was extracted and sent to Shanghai Gene-Pharma Co., Ltd. for mRNA sequencing. For details, see Supplementary Materials and Methods.

Apoptosis assay

The apoptosis assay was conducted using the fluorescein isothiocyanate (FITC) Annexin V Apoptosis Detection Kit with propidium iodide (PI; BioLegend, San Diego, CA, USA; 640914). The cells were washed cells twice with cold BioLegend Cell Staining Buffer, and then resuspend in Annexin V Binding Buffer at a concentration of 0.25–1.0 x 107 cells/mL. Then, 100 μL of cell suspension was transferred to a 5 mL test tube and 5 μL of FITC Annexin V was added, followed by 10 μL of PI solution. The cells were vortexed gently and incubated for 15 min at RT in the dark. Then, 400 μL of Annexin V Binding Buffer was added to each tube and the cells were analyzed using flow cytometry.

Wound healing assay

Cells were cultured to confluence in 6-well plates and wounded using a sterile pipette tip. The cell migration distance was observed by using an Olympus microscope (Olympus, Tokyo, Japan) and photographs were taken either immediately (0 h) and after 48 h of culture. Migration was quantified as the percentage of wound closure. The experiment was repeated at least three times independently.

Cell migration assay

Cells (5 × 104) in 200 μL of serum-free DMEM were seeded in the upper Transwell chambers (Costar, Corning, NY, USA, and DMEM containing 10% fetal bovine serum was added to the lower chamber as a

chemoattractant. After incubation at 37°C for 24 hours, cells that adhered to the lower surface were fixed with 100% methanol for 20 minutes at RT and subsequently stained with 0.1% crystal violet for 15 minutes. The assay was repeated at least three times independently.

Colony formation assay

A total of 400 treated GC cells (AGS or BGC-823) were seeded in a 6-well plates and incubated for 14 days. Then, the colonies were fixed with 100% methanol for 20 minutes at RT, stained with 0.1% crystal violet for 15 minutes, then cell colonies containing more than 50 cells were counted.

Cell invasion assay

Transwell chambers (6.5 mm, Costar) were pre-coated with Matrigel for 30 min. Then, Cells (1 × 105) in 200 μL of serum-free DMEM were seeded in the upper Transwell chambers, with DMEM containing 10% fetal bovine serum added to the lower chamber. After incubation at 37°C for 24 hours, cells that adhered to the lower surface were fixed with 100% methanol for 20 minutes at RT and subsequently stained with 0.1% crystal violet for 15 minutes. The assay was repeated at least three times independently.

Lipid staining assay

An Oil Red O stain kit (Nanjing Jiancheng Bioengineering Institute, Nanjing, China)) was used for neutral lipid staining. Briefly, cells were washed with PBS and incubated with Oil Red O solution for 15 min at RT. Cell nuclei were counterstained with 2 μg/mL 4',6-Diamidino-2-Phenylindole (DAPI) (BioFroxx, Einhausen, Germany; #1155MG010), and visualized under a fluorescence microscope. For confocal analysis, cells were fixed for 15 min in 4% formaldehyde/PBS, washed with 0.2% Triton-X 100/PBS, and incubated with BODIPY 493/503 (Thermo Fisher Scientific, D3922) and DAPI for 30 min and 5 min at room temperature, respectively.

Spheroid cell invasion assay

Spheroid cell invasion assay was performed using the 96 Well 3D Spheroid BME Cell Invasion Reagent Kit (Trevigen, MD, USA). Harvested BGC-823 cells were resuspended in 1 × Spheroid Formation ECM, and centrifuged at 200 g for 3 min at room temperature. Then, cells were incubated at 37°C in a tissue culture incubator for 72 h. 50 μl of invasion matrix was added per well, and plate was centrifuged at 300 g at 4°C for 5min. Plate was transferred to a tissue culture incubator set at 37°C for 1 h to promote gel formation. One hour later, 100 μl of cell culture medium containing chemoattractant and invasion modulating compounds was added, and was incubated at 37°C in a tissue culture incubator for 3–6 days. The spheroid in each well was photographed every 24 h using the ×4 objective. Images were analyzed to evaluate 3D culture cell invasion with Image J (http://rsb.info.nih.gov/ij/). BGC-823 cells were dyed with red fluoresce using DiL (Beyotime, Shanghai, China).

Peritoneal dissemination model

Male BALB/c nude mice (3–4 weeks old) were obtained from the Model Animal Research Center of Nanjing University and housed in a pathogen-free environment in the Animal Laboratory Unit of Nanjing

University. Peritoneal dissemination was evaluated through intraperitoneal injection. In brief, *APOC2* knockdown, *APOC2* overexpressing, and the corresponding control GC cells (3×10^6) in 400 μL of PBS were injected into the peritoneal cavity. PM (6 mice/group) was examined and recorded when the mice were sacrificed at 15 days after injection. All animal procedures were approved by the Nanjing Drum Tower Hospital Ethics Review Board (The Affiliated Hospital of Nanjing University School).

Statistical analysis

All statistical analyses were performed using SPSS software (version 19.0; IBM Corp., Armonk, NY, USA). All data are presented as the means ± standard deviation (SD). Student's t test was used to compare two groups. Frequencies of categorical variables were compared using the Pearson's χ^2 test. Survival curves were generated using the Kaplan–Meier method and compared using the log-rank test. Values of $P < 0.05$ were considered statistically significant.

Results

Quantitative proteomic analysis showed significant differences between GC tissues and Peritoneal metastasis Tissues

GC and PM types have not been compared systematically at the tissue proteomic level, and the differentiation between PM and primary GC is of fundamental clinical importance for therapeutic stratification; we explored the possibility of identifying biomarkers for proteomic diagnosis. The experimental process of the strategy used to identify the differentially expressed proteins (DEPs) in PM tissues is shown briefly in Fig. 1A. To find meaningful protein alterations in GC and PM tissues, we selected five patients diagnosed with advanced GC who had not received any treatment before surgery, and surgically extracted their tumor tissues and PM tissues for proteome profiling. A total of 759302 spectra were generated, and 46787 peptides and 7638 proteins were identified at 1% false discovery rate (FDR). This assay identified 7638 proteins with quantitative information (Supplementary Table 1). For the experimental design with more than one replicate, proteins with a 1.5 fold change and a P-value less than 0.05 were defined as differentially expressed proteins (DEPs). Compared with the primary GC, 595 proteins in the PM tissues were upregulated among these DEPs (Supplementary Table 2), while 1050 proteins were downregulated (Supplementary Table 3). Figure 1B briefly summarizes the identification results for the samples.

For gene ontology (GO) enrichment analysis, Blast2GO software was used to evaluate the functional significance of all identified proteins. Supplementary Table S4 and Figure S1A provide detailed protein-specific information and the visualization results, respectively. GO enrichment analysis indicated that the most abundant biological processes (among 28 GO terms) mainly included: 'cellular processes', 'metabolic processes'. The 'cell', 'cell part', and 'organelle' were the most enriched cell components (among 19 GO terms). The most enriched molecular functions (among 12 GO items) included: 'binding'

and ‘catalytic activity’. Next, we performed GO enrichment analysis on the identified DEPs (Supplementary Table 5). We drew a GO functional classification map to illustrate all DEPs (Fig. 1C) and distinguish between upregulated and downregulated proteins (Fig. 1D). We found that both upregulated and downregulated DEPs are involved in common structural or functional processes. However, some GO biological processes and molecular functions were specifically enriched for upregulated proteins (such as cell aggregation, protein tag) or downregulated proteins (such as nitrogen utilization, hijacked molecular function) (Fig. 1D). Next, we used the database of protein orthologs classification (EuKaryotic orthologous group (KOG)), to predict the potential functions of all identified proteins (Supplementary Table 6 and Figure S1B). And among the identified DEPs (Supplementary Table 7 and Fig. 1E), the most enriched KOG category was “cellular process and signal transduction", which showed that DEPs were mainly related to signal transduction mechanisms, post-translational modification, and protein renewal. Next, we performed Kyoto Encyclopedia of Genes and Genomes (KEGG) enrichment analysis on all identified proteins (Supplementary Table 8 and Figure S1C). Not only that, we further characterize the biologically functions involved involving these DEPs (Supplementary Table S8). The analysis showed that the upregulated proteins were related to 25 main pathways, of which ‘metabolic pathway’ was the most enriched category (Fig. 1F). Figure 1G shows the biological functions in the DEP set (Supplementary Table S9). The DEPs detected in our PM samples were mainly enriched in certain metabolic processes, especially biological processes related to lipid metabolism. Among them, ‘cholesterol metabolism’ was enriched in APOC2, LIPL, SORC2, IBP6, CD36, and APOA.

Correct protein sorting or protein targeting to the appropriate destination inside or outside the cell is essential; errors can cause illness. We predicted the subcellular localizations of the identified DEPs using bioinformatic tools (WoLF PSORT) (Fig. 1H). The analysis showed that intracellular, extracellular, and mitochondria were the most representative structures (see Supplementary Table 10 for the details). For the proteinprotein interaction network analysis, we used the STRING database (STRING 11.0) to analyze the DEPs to conduct network interaction analysis of protein-protein relationships within the first 100 confidence intervals (Figure I and Supplementary Table 11).

APOC2 was upregulated in patients with GC with PM

Through KEGG biological enrichment analysis, we found that the DEPs identified in our PM samples were mainly enriched in “regulation of lipid metabolic process”, “triglyceride catabolic process”, and “regulation of lipid catabolic process”, which ranked in the top 20 enriched biological processes. (Fig. 2A). The GSEA analysis also revealed that the DEPs identified in our PM samples were mainly enriched in “regulation of lipid metabolic process” related pathways (Fig. 2B). Therefore, we deduced that lipid metabolism might play an important role in PM. To further verify the association between the expression of lipid metabolism-related genes and the survival of patients with primary GC, we downloaded the latest transcriptome sequencing and clinical data of gastric cancer from The Cancer Genome Atlas (TCGA), including 375 cancer samples and 32 paracancerous samples. Then, we used the R package GSVA (version 1.36.2) to score a single sample of the TCGA Stomach Adenocarcinoma (TCGA-STAD) for this gene set. Next, we used the R package survminer (version 0.4.8) to determine the score to draw a survival

curve (Fig. 2C). We found that patients with GC with high expression of lipid metabolism genes had a poor survival prognosis, which further indicated that lipid metabolism might influence GC progression. To search for the possible core protein of lipid metabolism in PM, we visualized the fold change of proteins in the gene set of “regulation of lipid metabolic process” using a volcano plot, and found that APOC2 is highly expressed in PM from GC (Fig. 2D).

To further explore the mechanism of PM in GCs, we first examined the expression of APOC2 in GC cell lines and found that APOC2 was highly expressed in most GC cell lines (especially MKN-45, SNU-16, BGC-823, and AGS). However, the expression of APOC2 in GES1 cells, which are epithelial cells of the gastric mucosa, was very low (Fig. 2E). Then, we performed western blotting using surgical samples to explore APOC2 levels. In GC tissue, APOC2 levels were significantly higher than in adjacent normal gastric mucosal tissues (ANTs) and even PM lesions showed higher levels of APOC2(Fig. 2F). Immunohistochemistry (IHC) staining demonstrated that APOC2 was upregulated in GC tissues compared with that in the ANTs, and notably, APOC2 was expressed at significantly higher rates in PM tissues (Fig. 2G). IHC staining was used to measure APOC2 levels in a cohort containing 111 pairs of GC samples and matched ANTs. The clinicopathological features and complete follow-up data of these patients are summarized in Table 1. The patients were divided into low (score 0–2) or high (score 3–9) APOC2 groups according to staining intensity scores. Correlation analysis showed that high APOC2 expression in GC tissues correlated significantly with more aggressive tumor phenotypes. In addition, the high expression of APOC2 in GC tissue was related to the shortened overall survival (OS) time of patients (Fig. 2H). And according to APOC2 levels, we also assessed OS based on other major clinicopathological factors. Significant differences existed in T3-T4, a higher degree of lymphatic metastasis (N2-N3) and clinical stage III + IV tumors (Fig. 2I-K).

Knockdown of APOC2 inhibited the invasion, migration, proliferation, apoptosis resistance, and EMT of GC cells

To explore APOC2’s biological functions in GC, we chose two GC cell lines, AGS and BGC-823, which express APOC2 highly, as our cellular models. AGS and BGC-823 cells were transfected with control siRNA and *APOC2*-siRNAs (Si1, Si2, and Si3). At 72 h after treatment, the APOC2 mRNA and protein levels were determined, and siAPOC2#1 was shown to be the most efficient in downregulating APOC2 levels in both cell lines (Fig. 3A-D). Wound-healing, migration, invasion, clonal formation, and apoptosis assays to evaluate the influence of siAPOC2#1 on AGS and BGC-823 cells showed that the knockdown of *APOC2* significantly inhibited cell wound-healing (Fig. 3E, 3F), migration (Fig. 3G, 3H), invasion (Fig. 3G, 3H), clonal formation (Fig. 3I, 3J), and apoptosis resistance (Fig. 3K, 3L) compared with the siRNA control group. Moreover, *APOC2* knockdown effectively increased the levels of E-cadherin, but decreased N-cadherin and vimentin, Snail, Slug, Twist1, MMP-9, and MMP-2 levels in AGS and BGC-823 cells (Fig. 3M, 3N). These results indicated that high APOC2 expression could enhance the malignant phenotype of GC cells.

RNA-seq analysis revealed that knockdown of APOC2 inhibited PI3K/AKT/mTOR signaling and reduced the metabolic activity of GC cells

To further explore the regulatory mechanism of APOC2 in GC, we downloaded the relevant GC sequencing data from the TCGA database for analysis. According to the level of *APOC2* mRNA expression, we divided 375 GC tissue samples into two groups: APOC2_High (n = 188) and APOC2_Low (n = 187). Using R package limma to analyze the difference between the two sequencing datasets, we observed that APOC2 is mainly related to lipid absorption, transport, and metabolism of cells (Fig. 4A). AGS and BGC-823 cells were infected with lentivirus-shAPOC2 (to stably silence *APOC2*) and the control non-targeting shControl. Fluorescence (Fig. 4B) and western blotting (Fig. 4C) demonstrated the efficiency of lentiviral infection and knockdown in AGS and BGC-823 cells, respectively. We then performed transcriptome sequencing of AGS (n = 3) and AGS_shAPOC2 (n = 3) cells. The mRNA-seq analysis identified abundant gene expression changes after *APOC2* knockdown. Especially, those related to metabolic pathways were downregulated, such as lipid metabolism, cholesterol efflux, HDL particle remodeling, low density lipoprotein (LDL) particle remodeling, regulation of sterol transport, and reverse cholesterol transport (Fig. 4D, 4E). We also noted changes various signaling pathways, such as cancer pathways and the PI3K-AKT signaling pathway (Fig. 4F).

To clarify the molecular mechanism by which APOC2 regulates these lipid metabolism processes, we performed Oil Red O and BODIPY 493/503 staining to test whether APOC2 affects the formation of lipid droplet (LDs) in GC cells. *APOC2* knockdown significantly suppressed LD formation in AGS (Fig. 4G) and BGC-823 cells (Fig. 4H). *APOC2* knockdown also markedly inhibited the TC (Fig. 3I, 3J) and TG (Fig. 3K, 3L) synthesis in GC cells. These results suggested that APOC2 plays a key role in lipid metabolism and transportation, thus we speculated that regulating its expression in GC cells would affect their bioenergetic profile. We used Seahorse XF to measure the live-cell metabolic index and found that Lenti-shAPOC2#1 cells (AGS and BGC-823) exhibit lower energetic metabolic phenotype compared with Lenti-shControl cells (Fig. 3M). There was a decrease in mitochondrial respiration rates assessed by the oxygen consumption rates (OCR) was observed in shAPOC2 AGS cells at their basal conditions (Fig. 4N). But compared with shCtrl cells, shAPOC2 cells have a lower extracellular acidification rate (ECAR) under stress conditions (Fig. 4N).

The PI3K/AKT/mTOR axis plays a positive role in EMT and promotes tumor metastasis (27, 28). The role of the mTOR complex in lipid metabolism is particularly important (29). We next demonstrated that knockdown *APOC2* in AGS cells and BGC-823 cells decreased the levels of phosphorylated PI3K, AKT, and mTOR, but it barely affected total PI3K, AKT, and mTOR levels, which was consistent with the RNA-seq data (Fig. 3O, 3P). These data indicated that APOC2 is essential to regulate lipid metabolism and PI3K/AKT/mTOR signaling in GC cells.

The regulation by APOC2 of GC cell apoptosis, migration, invasion, proliferation and EMT was attributed to the PI3K/AKT/mTOR signaling pathway

Next, we explored whether APOC2 regulates the malignant phenotype through PI3K/AKT/mTOR signaling and clarified the signaling mechanism. Cell flow cytometry was used to test the effects of *APOC2* knockdown and the cell-permeable PI3K pathway activator 740Y-P on AGS and BGC-823 cell apoptosis. Compared with the siCtronl group, AGS and BGC-823 apoptosis in the siAPOC2 group increased significantly, while that in the 740Y-P group decreased significantly. However, 740Y-P could partially eliminate the effect of si-APOC2 transfection on GC cell apoptosis (Fig. 5A, 5B). Wound healing, migration, invasion, and the colony formation ability of GC cells were greatly reduced in the *APOC2* shRNA group and increased in the 740Y-P group, while 740Y-P restored the effects of *APOC2* knockdown (Fig. 5C–H). Similarly, 3D invasion assays showed that APOC2 silencing repressed BGC-823 cell invasion significantly, and 740Y-P abolished the effect of sh-APOC2 transfection on GC cell invasion (Fig. 5I-K).

Based on the above experimental results, we preliminarily verified that APOC2 has an important regulatory role in EMT, thereby affecting the malignant characteristics of GC cells, possibly via the PI3K/AKT/mTOR signaling pathway. Next, we confirmed the relevant effectors in this pathway using western blotting. The levels of p-PI3K, p-AKT, and p-mTOR were significantly decreased in the APOC2-shRNA group compared with those in the shCtrl group. After transfection with Lenti-shAPOC2, E-cadherin, a marker of epithelial cells, was upregulated, and N-cadherin, vimentin, Snail, Slug, Twist1, MMP-9, and MMP-2 were downregulated in AGS and BGC-823 cells (Fig. 6A, 6B). But treatment with 740YP had the opposite effects (Fig. 6A, 6B).

Lentiviral transfection was used to construct a GC cell line stably overexpressing *APOC2*. The efficiency of infection and overexpression in AGS and BGC-823 cells were verified by fluorescence and western blotting (Fig. 6C, 6D). The levels of p-PI3K, p-AKT, and p-mTOR were enhanced in *APOC2*-overexpressing AGS and MGC-803 cells. Overexpression of *APOC2* increased the levels of N-cadherin, vimentin, Snail, Slug, Twist1, MMP-9, and MMP-2 and decreased E-cadherin levels. GC cell treatment with LY294002, a selective inhibitor of PI3K-dependent AKT phosphorylation and kinase activity, inhibited PI3K-AKT-mTOR signaling and EMT of GC cells. Western blotting showed that *APOC2* overexpression induced E-cadherin downregulation and N-cadherin, vimentin, Snail, Slug, Twist1, MMP-9, MMP-2, p-PI3K, p-AKT and p-mTOR upregulation in AGS and BGC-823 cells, which was inhibited significantly by LY294002 (Fig. 6E, 6F).

In vivo validation of the role of APOC2 on PM of GC

To determine whether APOC2 could promote PM of GC cells, AGS-shControl and AGS shAPOC2 cells were injected into the peritoneal cavity of nude mice. Representative images of GC PM and H&E staining showing tumor progression in the peritoneum are presented in Fig. 7A. AGS shAPOC2 cells produced fewer PM nodules compared with those produce by AGS-shControl cells (Fig. 7C). The weight of the PM nodules in the AGS shAPOC2 group was also reduced significantly (Fig. 7D). In contrast, 740Y-P had the opposite effect on PM in vivo, and could partially reverse the impact of *APOC2* knockdown on peritoneal metastasis.

Furthermore, a PM model was established using *APOC2*-overexpressing AGS cells (Fig. 7B). As expected, *APOC2* overexpression increased the number (Fig. 7E) and weight (Fig. 7F) of the PM nodules. LY294002

inhibited PM of PC, which was enhanced by Lenti-oeAPOC2. Thus, we considered that PI3K inhibitor LY29004 might be used to inhibit the effect of APOC2. These data indicated that APOC2 promoted PM of GC through the PI3K/AKT/mTOR signaling pathway *in vivo*.

Discussion

Patients with PMs of GC have a poor quality of life, with a median survival of 7 months (30). Treatment options for patients with PM disease are limited, and temporary palliative treatment is mainly based on experience (31, 32). Therefore, molecular examination of PM is urgently needed to explore potential diagnostic and therapeutic targets.

RNA-seq and proteomics mass spectrometry studies were carried out to identify the transcriptional targets of tumorigenesis that lead to PM of GC (33–35). However, these sequencing samples mainly came from ascites or plasma of patients with PM from GC, which limited our understanding of the molecular or genomic composition of PM. To date PM nodule tissue has not been used for protein mass spectrometry sequencing to screen targets. Proteomics can provide a comprehensive and quantitative description of protein levels and their changes under the influence of biological interference, such as diseases or drug treatment (36). Tandem mass tag (TMT), an LC-MS/MS-based analysis strategy, is a powerful method for quantitative proteomics. It can identify proteins in different samples based on their relative abundance and quantify peptides and proteins using isotopomer labels, thereby creating large-scale, highly precise data sets with minimal missing values, and have been used widely quantitative proteomics (37–39). Therefore, detailed proteomic characterization of PM samples combined with transcriptomic analysis of GC cells could reveal changes in the drivers that promote PM development and progress.

In the present study, TMT-based proteomic analysis showed that 1600 proteins (595 upregulated and 1065 downregulated) were differentially abundant between GC and PM tissues. Bioinformatic analysis of the DEPs showed that the upregulated proteins in PM tissues were mainly related to lipid metabolism and tumor extracellular matrix components. Further R-language-based analysis demonstrated that APOC2 was highly expressed in PMs and played a central role in lipid metabolism. Paget's "seed and soil" theory of tumorigenesis is a widely known theory of PM (40, 41). Metastatic homing of malignant cells is governed by interactions between metastatically competent cancer cells (“seed”) and the permissive microenvironment of specific organs (“soil”) (42). Cancer cells are expected to show higher energy requirements than healthy gastric mucosal cells to achieve their increased invasion potential (43, 44). The relationship between lipid metabolism and cancer has been proven; however, there are relatively few reports on the role of APOC2 in cancer. APOC2 is an important component of LDL, VLDL, and HDL, where it helps to hydrolyze triglycerides related to lipoproteins via its ability to activate LPL (45). APOC2 has been demonstrated to be closely associated with survival of patients with pancreatic cancer (46). Pancreatic cancer cells with high APOC2 expression show enhanced cell invasion capability. Elevated APOC2 levels have been considered to be of diagnostic importance (47) and associated with pancreatic cancer-associated cachexia (48). In addition, APOC2 could be used as a potential serum biomarker to

predict and estimate the radiation treatment outcome of patients with locally advanced cervical cancer (49). APOC2 levels in gastrointestinal stromal tumor tissues were significantly higher than those in adjacent normal tissues. Inhibiting *APOC2* expression inhibited the invasion of gastrointestinal stromal tumor (GIST) cells (50). APOC2 is also highly expressed in acute myeloid leukemia and is associated with poor clinical outcomes. In addition, APOC2 promotes the growth of leukemia through the CD36-ERK signaling pathway (18). These studies indicated that APOC2 plays an important role in cancer cells; however, we lack a detailed explanation of its mechanism in these diseases. Therefore, we hypothesized that high APOC2 expression could maintain the metabolic requirements of GC cells to further promote their metastasis to peritoneal tissues.

We verified that APOC2 levels were not only high in GC cells, but also higher in patients' PMs tissues compared with that in primary GC tissues. Investigating the clinical importance of APOC2 in 111 patients GC showed that APOC2 correlated positively with GC progression. In addition, Kaplan-Meier survival curve analysis showed that the overall survival of patients with high APOC2 expression was much shorter than that of patients with low APOC2 expression. Moreover, the assessment of the prognostic significance of APOC2 expression based on clinicopathological factors identified significant differences in patients with T3-T4 disease and lymph node metastasis. Thus, APOC2 correlated markedly with shorter survival of patients with a more aggressive tumor phenotype, indicating that APOC2 could be used as a prognostic indicator for patients with GC (Table 1). The proteomics data showed that extracellular matrix components related to the DEPs are highly expressed in GC PM tissue, and previous studies showed that EMT is critical for the development of cancer via the transformation of epithelial cells into mesenchymal cells to promote tumor cell metastasis (51). Interestingly, when *APOC2* was knocked down in GC cells, the malignant phenotypes of the GC cells and the expression of EMT markers were inhibited.

To further explore APOC2's mechanism in the process of GC PM, we knocked down APOC2 in GC cell lines and then performed RNA-sEq. KEGG pathway enrichment analysis showed that *APOC2* knockdown in GC cell lines caused changes in certain lipid metabolism pathways, such as cholesterol, and affected the PI3K/AKT/MTOR signaling pathway. Our study showed that APOC2 was responsible for the formation of LDs in GC cells, and *APOC2* knockdown in GC cells not only inhibited the synthesis of TCs and TGs but also affected the energy metabolism phenotype of GC cells. PI3K/AKT/mTOR signals play a key role in the EMT process (52, 53). EMT involves a transition from the expression of the epithelial marker E-cadherin to a cell state that favors the expression of mesenchymal markers, including N-cadherin and vimentin (54). These changes are manifested at the transcription level by regulating the activity of EMT transcription factors (such as Snail, Slug and Twist1) (55). Therefore, we explored the potential of the PI3K/AKT/mTOR pathway to participate in APOC2-mediated EMT of GC cells. The results showed that knocking down *APOC2* down-regulates the PI3K/AKT/mTOR pathway, thereby inhibiting EMT and inhibiting the migration and invasion of GC cells. However, 740Y-P could partially reverse the effects of *APOC2* knockdown on the malignant phenotypes of GC cells *in vivo* and *in vitro*. Similarly, overexpression of *APOC2* activated the PI3K/AKT/MTOR and EMT pathways, and increased the levels of MMP2 and MMP9 proteins, thereby increasing the migration, invasion, and metastasis ability of GC cells

in vivo and *in vitro*. And the effect of overexpression of APOC2 was partially reversed using the PI3K inhibitor, LY29004.

Conclusions

In summary, we determined the proteomic alterations between GC and PM samples, and combined with GC cell transcriptomics analysis, we found that APOC2 regulated the EMT of GC cells through the PI3K/AKT/mTOR signaling pathway that promotes the transfer of GC cells to the peritoneum. Therefore, the APOC2 and PI3K/AKT/mTOR pathways might serve as targets for new treatment strategies for GC peritoneal metastasis.

Abbreviations

PM: Peritoneal metastasis; GC: gastric cancer; APOC2: Apolipoprotein C-II; IHC: immunohistochemistry; LC-MS/MS: liquid chromatography-tandem mass spectrometry; EMT: Epithelial to mesenchymal transition; PI3K: phosphoinositide 3-kinase; AKT: protein kinase B; mTOR: mammalian target of rapamycin.

Declarations

Acknowledgements

Not applicable.

Authors' contributions

W.G. and S.L designed the study. C.W., Z.Y. and E.X. performed the experiments. C.W and Z.Y. collected the data. C.W., X.W., Z.L., K.C. and H.Y. analyzed and interpreted the data. C.W. and S.L. wrote the manuscript. All authors read and approved the final manuscript.

Funding

This work was supported by the Natural Science Foundation of Jiangsu Province (BK 20200052), the National Natural Science Foundation of China [grant number 81602103]; the Distinguished Young Scholar Project of Medical Science and Technology Development Foundation of Nanjing Department of Health [grant number JQX17005]; and the Wu Jieping Medical Foundation [grant number 320.2710.1817].

Availability of data and materials

The data supporting the conclusions of this study are included in this paper and its additional files.

Ethics approval and consent to participate

The use of the clinical samples was approved by the Hospital Ethics Committee of Nanjing Drum Tower Hospital (The Affiliated Hospital of Nanjing University School) and carried out in accordance with the principles of the Declaration of Helsinki. All animal procedures were approved by the Nanjing Drum Tower Hospital Ethics Review Board (The Affiliated Hospital of Nanjing University School).

Consent for publication

All contributing authors agree to the publication of this article.

Competing interests

The authors declare that they have no known competing interests.

Author details

[1]Department of General Surgery, Nanjing Drum Tower Hospital, The Affiliated Hospital of Nanjing University School, Nanjing 210008, China; [2]Department of General Surgery, Nanjing Drum Tower Hospital Clinical College of Nanjing Medical University, Nanjing 210008, China.

References

1. Bray F, Ferlay J, Soerjomataram I, Siegel RL, Torre LA, Jemal A. Global cancer statistics 2018: GLOBOCAN estimates of incidence and mortality worldwide for 36 cancers in 185 countries. CA Cancer J Clin. 2018;68(6):394-424.
2. Chen W, Zheng R, Baade PD, Zhang S, Zeng H, Bray F, et al. Cancer statistics in China, 2015. CA Cancer J Clin. 2016;66(2):115-32.
3. Ji L, Selleck MJ, Morgan JW, Xu J, Babcock BD, Shavlik D, et al. Gastric Cancer Peritoneal Carcinomatosis Risk Score. Ann Surg Oncol. 2020;27(1):240-7.
4. Manzanedo I, Pereira F, Rihuete Caro C, Pérez-Viejo E, Serrano Á, Gutiérrez Calvo A, et al. Cytoreductive Surgery and Hyperthermic Intraperitoneal Chemotherapy (HIPEC) for Gastric Cancer with Peritoneal Carcinomatosis: Multicenter Study of Spanish Group of Peritoneal Oncologic Surgery (GECOP). Ann Surg Oncol. 2019;26(8):2615-21.
5. Kobayashi D, Kodera Y. Intraperitoneal chemotherapy for gastric cancer with peritoneal metastasis. Gastric Cancer. 2017;20(Suppl 1):111-21.
6. Dong D, Tang L, Li ZY, Fang MJ, Gao JB, Shan XH, et al. Development and validation of an individualized nomogram to identify occult peritoneal metastasis in patients with advanced gastric cancer. Ann Oncol. 2019;30(3):431-8.
7. Alyami M, Hübner M, Grass F, Bakrin N, Villeneuve L, Laplace N, et al. Pressurised intraperitoneal aerosol chemotherapy: rationale, evidence, and potential indications. Lancet Oncol. 2019;20(7):e368-e77.

8. LaRosa JC, Levy RI, Herbert P, Lux SE, Fredrickson DS. A specific apoprotein activator for lipoprotein lipase. Biochem Biophys Res Commun. 1970;41(1):57-62.
9. Lusis AJ, Heinzmann C, Sparkes RS, Scott J, Knott TJ, Geller R, et al. Regional mapping of human chromosome 19: organization of genes for plasma lipid transport (APOC1, -C2, and -E and LDLR) and the genes C3, PEPD, and GPI. Proceedings of the National Academy of Sciences of the United States of America. 1986;83(11):3929-33.
10. Smit M, van der Kooij-Meijs E, Frants RR, Havekes L, Klasen EC. Apolipoprotein gene cluster on chromosome 19. Definite localization of the APOC2 gene and the polymorphic Hpa I site associated with type III hyperlipoproteinemia. Hum Genet. 1988;78(1):90-3.
11. Lenich C, Brecher P, Makrides S, Chobanian A, Zannis VI. Apolipoprotein gene expression in the rabbit: abundance, size, and distribution of apolipoprotein mRNA species in different tissues. J Lipid Res. 1988;29(6):755-64.
12. Zannis VI, Cole FS, Jackson CL, Kurnit DM, Karathanasis SK. Distribution of apolipoprotein A-I, C-II, C-III, and E mRNA in fetal human tissues. Time-dependent induction of apolipoprotein E mRNA by cultures of human monocyte-macrophages. Biochemistry. 1985;24(16):4450-5.
13. Wu AL, Windmueller HG. Relative contributions by liver and intestine to individual plasma apolipoproteins in the rat. J Biol Chem. 1979;254(15):7316-22.
14. Goldberg IJ, Scheraldi CA, Yacoub LK, Saxena U, Bisgaier CL. Lipoprotein ApoC-II activation of lipoprotein lipase. Modulation by apolipoprotein A-IV. J Biol Chem. 1990;265(8):4266-72.
15. Kei AA, Filippatos TD, Tsimihodimos V, Elisaf MS. A review of the role of apolipoprotein C-II in lipoprotein metabolism and cardiovascular disease. Metabolism: clinical and experimental. 2012;61(7):906-21.
16. Musliner TA, Herbert PN, Church EC. Activation of lipoprotein lipase by native and acylated peptides of apolipoprotein C-II. Biochim Biophys Acta. 1979;573(3):501-9.
17. Zhang T, Yang J, Vaikari VP, Beckford JS, Wu S, Akhtari M, et al. Apolipoprotein C2 - CD36 Promotes Leukemia Growth and Presents a Targetable Axis in Acute Myeloid Leukemia. Blood Cancer Discovery. 2020;1(2):198-213.
18. Gao M, Yang C, Wang X, Guo M, Yang L, Gao S, et al. ApoC2 deficiency elicits severe hypertriglyceridemia and spontaneous atherosclerosis: A rodent model rescued from neonatal death. Metabolism: clinical and experimental. 2020;109:154296.
19. Yang C, Tian W, Ma S, Guo M, Lin X, Gao F, et al. AAV-Mediated ApoC2 Gene Therapy: Reversal of Severe Hypertriglyceridemia and Rescue of Neonatal Death in ApoC2-Deficient Hamsters. Mol Ther Methods Clin Dev. 2020;18:692-701.
20. Lamouille S, Xu J, Derynck R. Molecular mechanisms of epithelial-mesenchymal transition. Nat Rev Mol Cell Biol. 2014;15(3):178-96.
21. Yue B, Song C, Yang L, Cui R, Cheng X, Zhang Z, et al. METTL3-mediated N6-methyladenosine modification is critical for epithelial-mesenchymal transition and metastasis of gastric cancer. Molecular cancer. 2019;18(1):142.

22. Dong J, Wang R, Ren G, Li X, Wang J, Sun Y, et al. HMGA2-FOXL2 Axis Regulates Metastases and Epithelial-to-Mesenchymal Transition of Chemoresistant Gastric Cancer. Clin Cancer Res. 2017;23(13):3461-73.
23. Li T, Huang H, Shi G, Zhao L, Li T, Zhang Z, et al. TGF-β1-SOX9 axis-inducible COL10A1 promotes invasion and metastasis in gastric cancer via epithelial-to-mesenchymal transition. Cell death & disease. 2018;9(9):849.
24. Chang L, Graham PH, Hao J, Ni J, Bucci J, Cozzi PJ, et al. Acquisition of epithelial-mesenchymal transition and cancer stem cell phenotypes is associated with activation of the PI3K/Akt/mTOR pathway in prostate cancer radioresistance. Cell death & disease. 2013;4:e875.
25. Yin T, Wang G, He S, Shen G, Su C, Zhang Y, et al. Malignant Pleural Effusion and ascites Induce Epithelial-Mesenchymal Transition and Cancer Stem-like Cell Properties via the Vascular Endothelial Growth Factor (VEGF)/Phosphatidylinositol 3-Kinase (PI3K)/Akt/Mechanistic Target of Rapamycin (mTOR) Pathway. J Biol Chem. 2016;291(52):26750-61.
26. Zhang X, Wang S, Wang H, Cao J, Huang X, Chen Z, et al. Circular RNA circNRIP1 acts as a microRNA-149-5p sponge to promote gastric cancer progression via the AKT1/mTOR pathway. Molecular cancer. 2019;18(1):20.
27. Mossmann D, Park S, Hall MN. mTOR signalling and cellular metabolism are mutual determinants in cancer. Nat Rev Cancer. 2018;18(12):744-57.
28. Caron A, Richard D, Laplante M. The Roles of mTOR Complexes in Lipid Metabolism. Annu Rev Nutr. 2015;35:321-48.
29. Rau B, Brandl A, Piso P, Pelz J, Busch P, Demtröder C, et al. Peritoneal metastasis in gastric cancer: results from the German database. Gastric Cancer. 2020;23(1):11-22.
30. Rau B, Brandl A, Thuss-Patience P, Bergner F, Raue W, Arnold A, et al. The efficacy of treatment options for patients with gastric cancer and peritoneal metastasis. Gastric Cancer. 2019;22(6):1226-37.
31. Chia CS, You B, Decullier E, Vaudoyer D, Lorimier G, Abboud K, et al. Patients with Peritoneal Carcinomatosis from Gastric Cancer Treated with Cytoreductive Surgery and Hyperthermic Intraperitoneal Chemotherapy: Is Cure a Possibility? Ann Surg Oncol. 2016;23(6):1971-9.
32. Jin J, Son M, Kim H, Kim H, Kong S-H, Kim HK, et al. Comparative proteomic analysis of human malignant ascitic fluids for the development of gastric cancer biomarkers. Clin Biochem. 2018;56:55-61.
33. Tokuhisa M, Ichikawa Y, Kosaka N, Ochiya T, Yashiro M, Hirakawa K, et al. Exosomal miRNAs from Peritoneum Lavage Fluid as Potential Prognostic Biomarkers of Peritoneal Metastasis in Gastric Cancer. PloS one. 2015;10(7):e0130472.
34. Zhao J, Qin R, Chen H, Yang Y, Qin W, Han J, et al. A nomogram based on glycomic biomarkers in serum and clinicopathological characteristics for evaluating the risk of peritoneal metastasis in gastric cancer. Clin Proteomics. 2020;17:34.

35. Anderson NL, Anderson NG. Proteome and proteomics: new technologies, new concepts, and new words. Electrophoresis. 1998;19(11):1853-61.
36. Moulder R, Bhosale SD, Goodlett DR, Lahesmaa R. Analysis of the plasma proteome using iTRAQ and TMT-based Isobaric labeling. Mass Spectrom Rev. 2018;37(5):583-606.
37. Myers SA, Klaeger S, Satpathy S, Viner R, Choi J, Rogers J, et al. Evaluation of Advanced Precursor Determination for Tandem Mass Tag (TMT)-Based Quantitative Proteomics across Instrument Platforms. J Proteome Res. 2019;18(1):542-7.
38. Thompson A, Schäfer J, Kuhn K, Kienle S, Schwarz J, Schmidt G, et al. Tandem mass tags: a novel quantification strategy for comparative analysis of complex protein mixtures by MS/MS. Anal Chem. 2003;75(8):1895-904.
39. Fidler IJ. The pathogenesis of cancer metastasis: the 'seed and soil' hypothesis revisited. Nat Rev Cancer. 2003;3(6):453-8.
40. Akhtar M, Haider A, Rashid S, Al-Nabet ADMH. Paget's "Seed and Soil" Theory of Cancer Metastasis: An Idea Whose Time has Come. Adv Anat Pathol. 2019;26(1):69-74.
41. Mikuła-Pietrasik J, Uruski P, Tykarski A, Książek K. The peritoneal "soil" for a cancerous "seed": a comprehensive review of the pathogenesis of intraperitoneal cancer metastases. Cellular and molecular life sciences : CMLS. 2018;75(3):509-25.
42. Liu Q, Luo Q, Halim A, Song G. Targeting lipid metabolism of cancer cells: A promising therapeutic strategy for cancer. Cancer letters. 2017;401:39-45.
43. Xiang J, Liu L, Wang W, Xu H, Wu C, Xu J, et al. Metabolic tumor burden: a new promising way to reach precise personalized therapy in PDAC. Cancer letters. 2015;359(2):165-8.
44. Wolska A, Dunbar RL, Freeman LA, Ueda M, Amar MJ, Sviridov DO, et al. Apolipoprotein C-II: New findings related to genetics, biochemistry, and role in triglyceride metabolism. Atherosclerosis. 2017;267:49-60.
45. Xue A, Chang JW, Chung L, Samra J, Hugh T, Gill A, et al. Serum apolipoprotein C-II is prognostic for survival after pancreatic resection for adenocarcinoma. Br J Cancer. 2012;107(11):1883-91.
46. Chen J, Anderson M, Misek DE, Simeone DM, Lubman DM. Characterization of apolipoprotein and apolipoprotein precursors in pancreatic cancer serum samples via two-dimensional liquid chromatography and mass spectrometry. J Chromatogr A. 2007;1162(2):117-25.
47. Felix K, Fakelman F, Hartmann D, Giese NA, Gaida MM, Schnölzer M, et al. Identification of serum proteins involved in pancreatic cancer cachexia. Life Sci. 2011;88(5-6):218-25.
48. Harima Y, Ikeda K, Utsunomiya K, Komemushi A, Kanno S, Shiga T, et al. Apolipoprotein C-II is a potential serum biomarker as a prognostic factor of locally advanced cervical cancer after chemoradiation therapy. International journal of radiation oncology, biology, physics. 2013;87(5):1155-61.
49. Chen Y, Qin C, Cui X, Geng W, Xian G, Wang Z. miR-4510 acts as a tumor suppressor in gastrointestinal stromal tumor by targeting APOC2. J Cell Physiol. 2020;235(7-8):5711-21.

50. Bure IV, Nemtsova MV, Zaletaev DV. Roles of E-cadherin and Noncoding RNAs in the Epithelial-mesenchymal Transition and Progression in Gastric Cancer. International journal of molecular sciences. 2019;20(12).
51. Wang J, Jiang C, Li N, Wang F, Xu Y, Shen Z, et al. The circEPSTI1/mir-942-5p/LTBP2 axis regulates the progression of OSCC in the background of OSF via EMT and the PI3K/Akt/mTOR pathway. Cell death & disease. 2020;11(8):682.
52. Shao Q, Zhang Z, Cao R, Zang H, Pei W, Sun T. CPA4 Promotes EMT in Pancreatic Cancer via Stimulating PI3K-AKT-mTOR Signaling. Onco Targets Ther. 2020;13:8567-80.
53. Brabletz T, Kalluri R, Nieto MA, Weinberg RA. EMT in cancer. Nat Rev Cancer. 2018;18(2):128-34.
54. De Craene B, Berx G. Regulatory networks defining EMT during cancer initiation and progression. Nat Rev Cancer. 2013;13(2).

Tables

Due to technical limitations, table 1 is only available as a download in the Supplemental Files section.

Figures

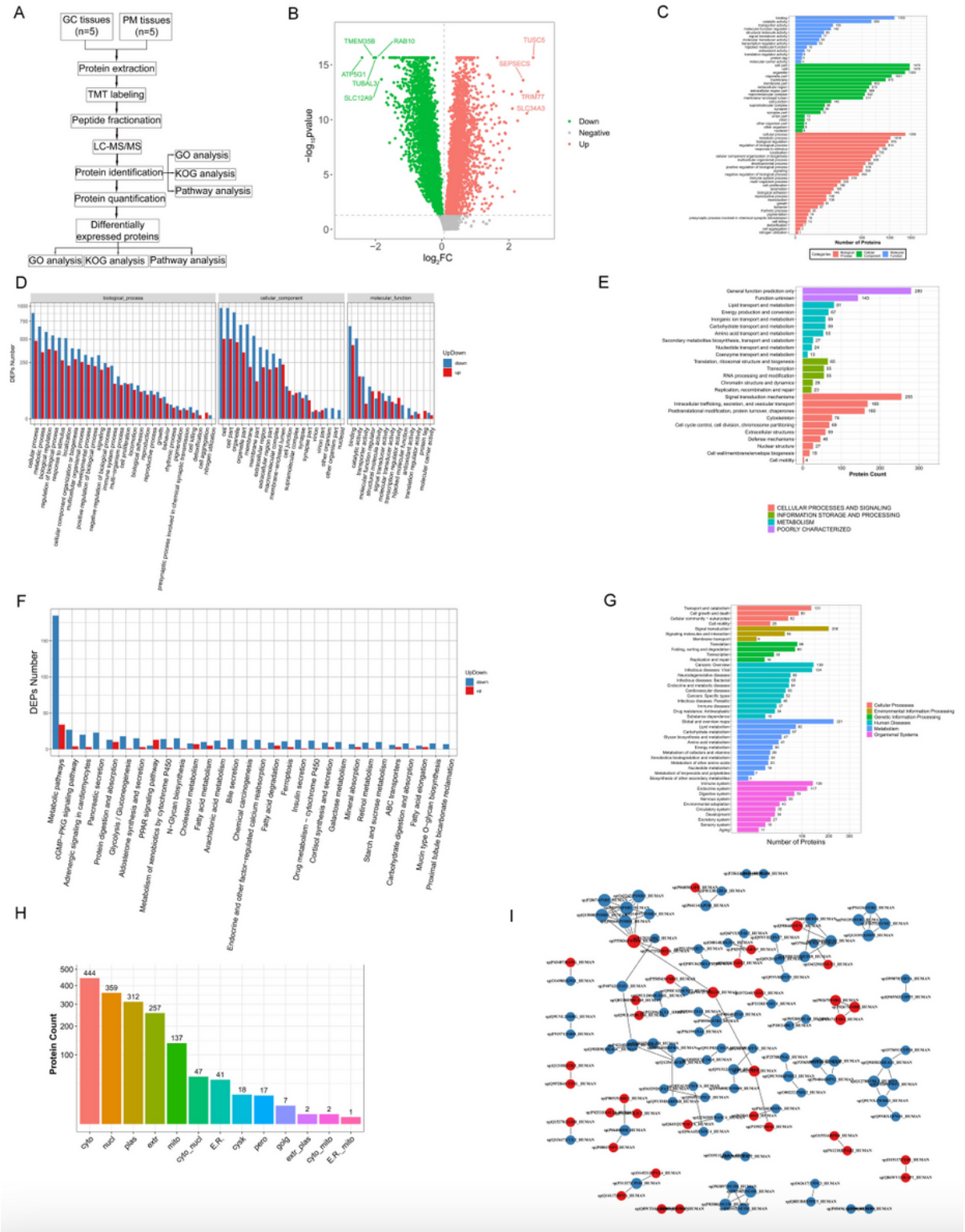

Figure 1

Analysis of DEPs between GC tissue and PM tissue based on TMT-labeled quantitative proteomics. (A) Schematic diagram of the workflow for the discovery and verification of cancer biomarkers for patients with GC with PM. (B) 595 proteins were upregulated and 1050 proteins were downregulated in PM samples compared with GC tissues. (C) GO enrichment analysis of all the DEPS. (D) GO classification of up- and downregulated DEPs. (E) The potential functions of DEPs annotated by KOG. (F) KEGG pathway

classification of up- and downregulated DEPs. (G) KEGG enrichment analysis to characterize the biological functions of the DEPs. (H) The subcellular localization of the identified DEPs. (I) Network interaction analysis of protein-protein relationships.

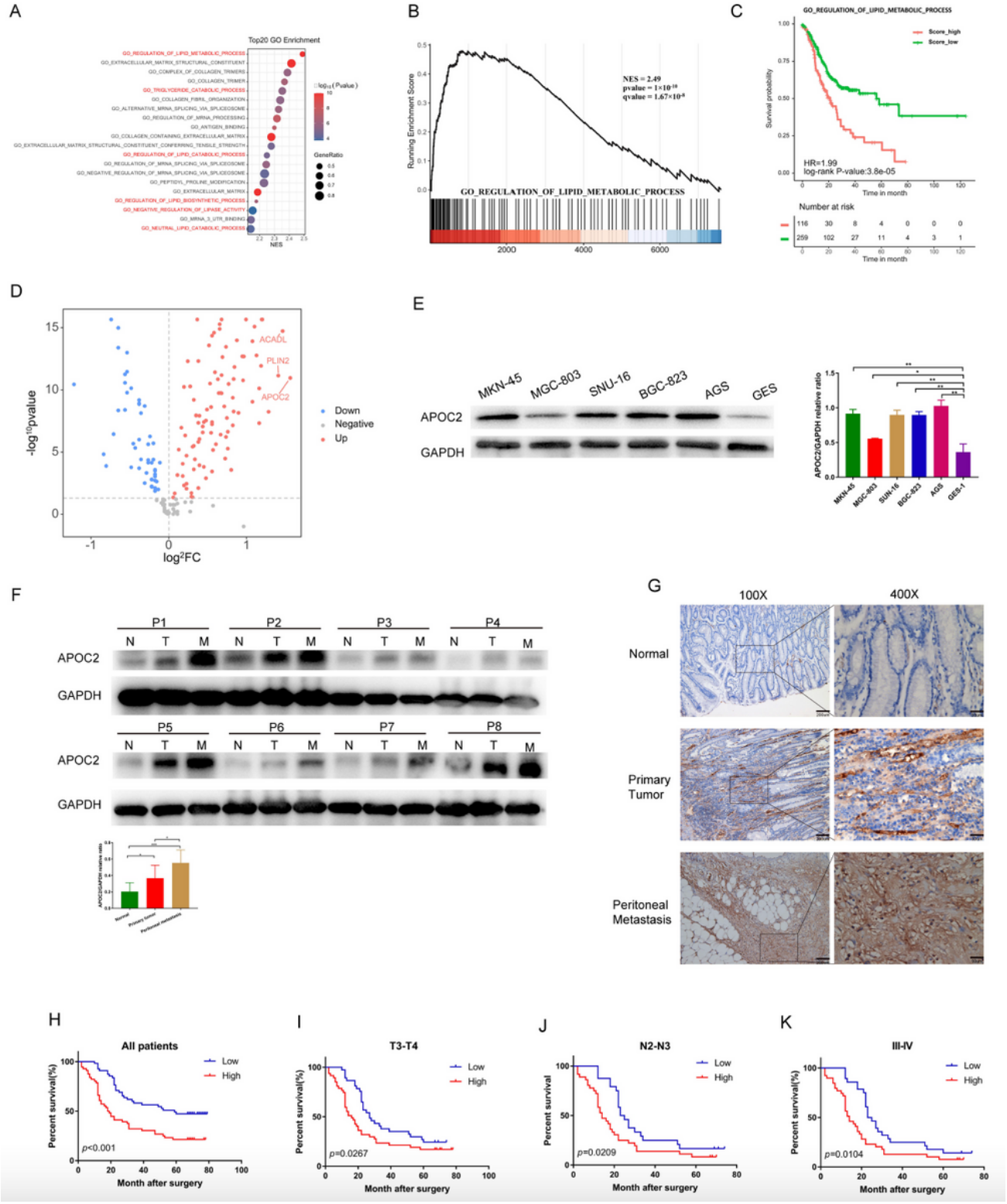

Figure 2

APOC2 was upregulated in GC patients with PM. (A) The DEPs identified in our PM samples were mainly related to the biological process of lipid metabolism. (B) GSEA analysis revealed that the DEPs identified

in our PM samples were mainly enriched in “regulation of lipid metabolic process” pathway. (C) GC Patients with high expression of lipid metabolism genes have a poor survival prognosis. (D) A volcano plot showing that APOC2 is highly expressed in the PM tissues from patients with GC. (E) Western blotting analysis of APOC2 protein levels in various GC cell lines and normal gastric epithelial cell line GES-1. Each experiment was repeated at least three times. Data represent mean ± SD, *P < 0.05, **P < 0.01, based on Student’s t-test. (F) Western blotting analysis of APOC2 levels from six patients with GC in tumor tissues (T) and matched adjacent non-cancerous gastric tissues (ANTs) (N), and PM (M). Each experiment was repeated at least three times. Data represent mean ± SD, *P < 0.05, **P < 0.01, ***P < 0.001, based on Student’s t-test. (G) Immunohistochemical staining analysis of APOC2 protein levels in patients with GC with primary tumor tissues and matched omental metastatic lesions. Representative images of APOC2 levels in ANTs, GC tissues, and GC PM tissues are shown. (H-K) Kaplan–Meier analysis of overall survival of patients with GC according to APOC2 expression in GC tissues (n = 111) and normal controls (n = 111).

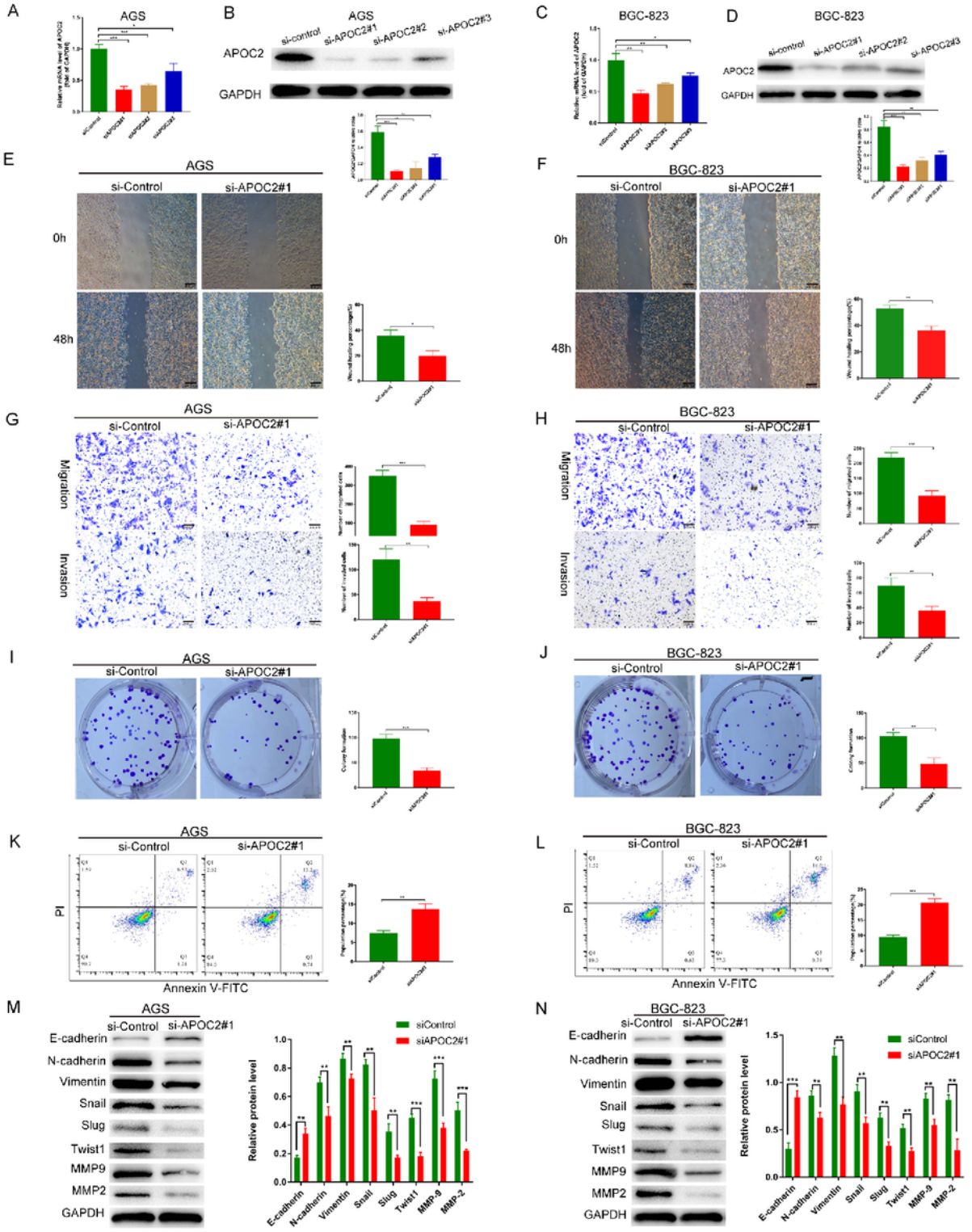

Figure 3

Knockdown of APOC2 expression inhibited the malignant phenotype of GC cells, including EMT. (A-D) PCR and Western blotting were used to evaluate the knockout efficiency of the APOC2-specific small interfering RNAs (siRNAs) (siAPOC2#1, siAPOC2#2, and siAPOC2#3) in AGS and BGC-823 cells. (E, F) Cell mobility analyzed using a wound healing assay. (G-H) migration and invasion of siAPOC2#1 and siControl cells were detected using Transwell migration and invasion assays. (I, J) Colony formation

assay of AGS and BGC-823 cells transfected with siAPOC2#1 and siControl. (K, L) Propidium iodide (PI) and Annexin V staining levels were determined by flow cytometry to assess cell apoptosis in AGS and BGC-823 cells transfected with siAPOC2#1 and siControl. (M, N) The protein levels of E-cadherin, N cadherin, vimentin, Snail, Slug, Twist1, MMP-9, and MMP-2 in AGS and BGC-823 cells transfected with siAPOC2#1 and siControl. Data are shown as mean ± SD; *P < 0.05, **P < 0.01, ***P < 0.001, based on Student's t-test.

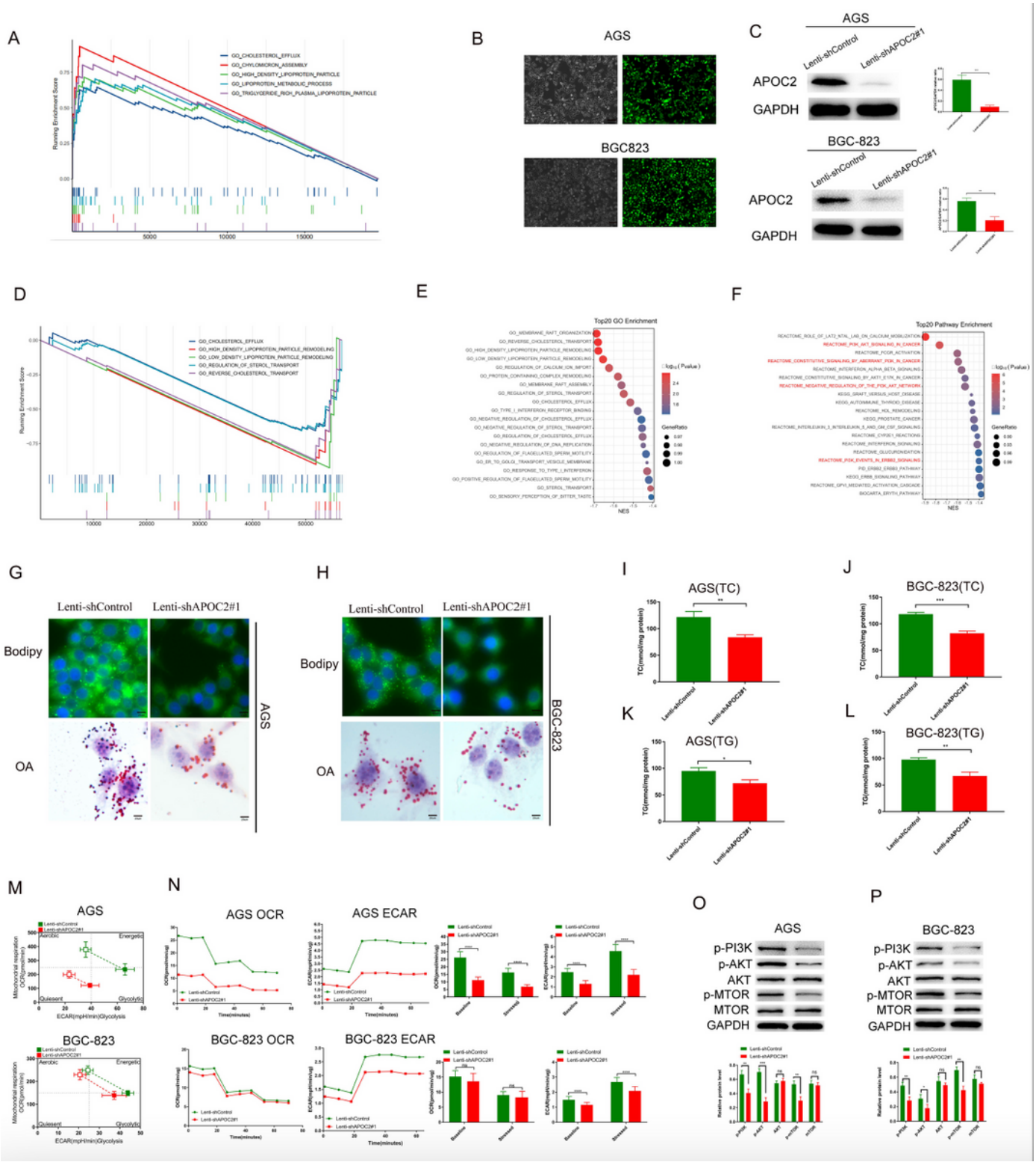

Figure 4

Knockdown of APOC2 expression in GC cells inhibited the PI3K/AKT/mTOR signaling pathway and lipid metabolic. (A). APOC2 was mainly related to the lipid absorption, transport, and metabolism of cells. (B, C) Fluorescence and western blotting were used to assesses the efficiency of lentiviral infection and knockdown of APOC2 in AGS and BGC-823 cells, respectively. (D, E, F). GSEA was used to analyze and interpret cellular pathway-level alterations in mRNA sequencing experiments. (G, H) Representative images of lipid droplets (LDs) in AGS and BGC-823 cells transfected with Lenti-shAPOC2#1 and Lenti-shControl as evaluated using BODIPY 493/503 staining (green) and Oil Red O staining; cell nuclei were stained with 4',6-Diamidino-2-Phenylindole(DAPI) (blue). (I, J) Concentration of total cholesterols (TCs) in AGS and BGC-823 cells transfected with Lenti-shAPOC2#1 and Lenti-shControl. (K, L) Concentration of triglyceride (TGs) in AGS and BGC-823 cells transfected with Lenti shAPOC2#1 and Lenti-shControl. (M) Cell energy phenotype of Lenti-shAPOC2#1 and Lenti-shControl AGS and BGC-823 cells. Baseline phenotype is indicated by an open marker. Stressed phenotype is indicated by a filled marker. (N) The oxygen consumption rate (OCR) and extracellular acidification rate (ECAR) of AGS and BGC-823 cells transfected with Lenti-shAPOC2#1 and Lenti-shControl tested by Seahorse XF cell analysis. (O, P) After the cells were transfected with Lenti-shAPOC2#1 and Lenti-shControl, the proteins in the PI3K/AKT/mTOR pathway of AGS and BGC-823 cells were evaluated using western blotting. Data are shown as mean ± SD; ns: no significant difference; *P < 0.05, **P < 0.01, ***P < 0.001, ****P < 0.0001, based on Student’s t-test.

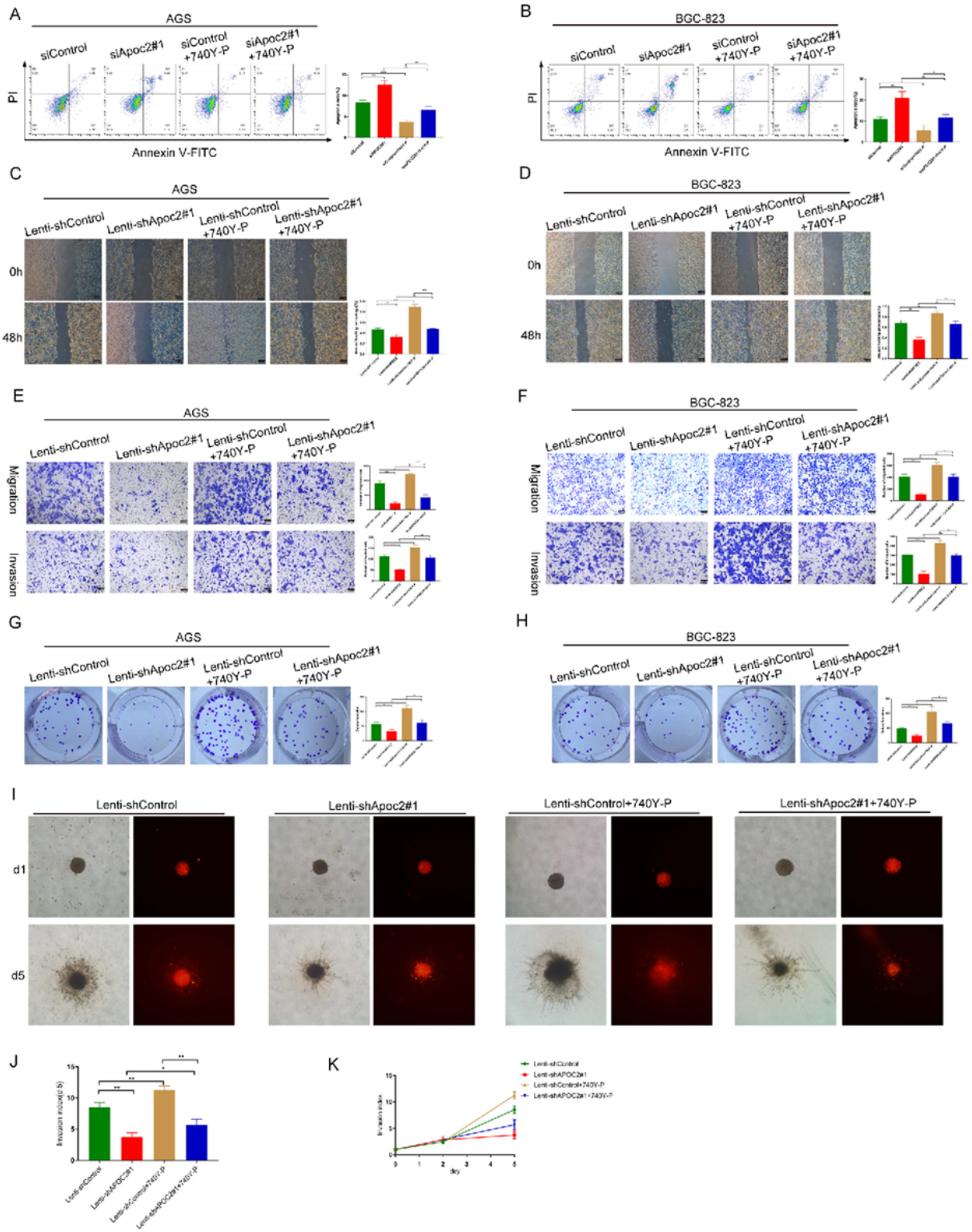

Figure 5

Inhibition of APOC2 reduced gastric cancer (GC) cell migration, invasion, proliferation, and increased apoptosis. (A, B) Flow cytometry was used to assess cellular apoptosis, with or without APOC2 inhibition, in GC cells, as well as with or without the PI3K pathway activator by 740Y-P. (C–H) Wound healing, Transwell, and colony formation assays were performed to detect the migration, invasion, and proliferation ability of GC cells transfected with Lenti-shAPOC2#1 and Lenti-shControl, as well as those of

cells with or without 740Y-P. (I-K) 3D invasion assays revealed that APOC2 silencing repressed BGC-823 invasion significantly, and 740Y-P abolished the effect of Lenti-shAPOC2 transfection on GC cell Invasion ability. Data represent mean ± SD. of three independent experiments. The level of significance is indicated by *P < 0.05, **P < 0.01, ***P < 0.001.

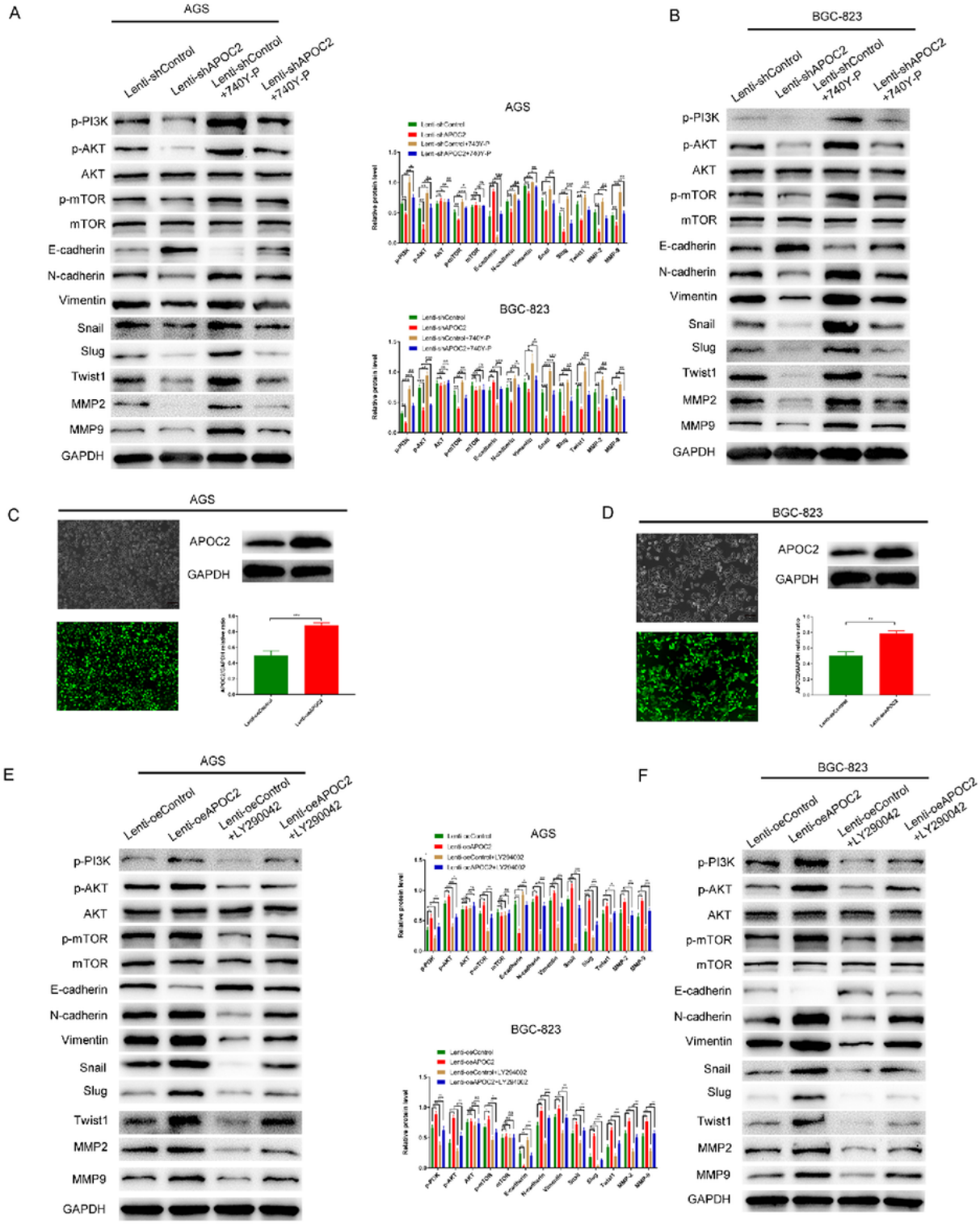

Figure 6

APOC2 mediated EMT and PI3K/AKT/mTOR signaling in GC cells. (A, B) The protein levels of p-PI3K, p-AKT, p-mTOR, E cadherin, N-cadherin, vimentin, Snail, Slug, Twist1, MMP-9, and MMP-2 in GC cells transfected with Lenti-shAPOC2#1 and Lenti-shControl, as well as cells with or without the PI3K pathway activator 740Y-P. (C, D) Fluorescence and western blot were used to assesses the efficiency of lentiviral infection and overexpression of APOC2 in AGS and BGC-823 cells, respectively. (E, F). The protein level of p-PI3K, p-AKT, p-mTOR, E-cadherin, N-cadherin, vimentin, Snail, Slug, Twist1, MMP-9, and MMP-2 in AGS and BGC-823 cells transfected with Lenti-shAPOC2#1 and Lenti-shControl, as well as cells with or without PI3K pathway inhibitor by LY294002. Data represent mean ± SD. of three independent experiments. The level of significance is indicated by *P < 0.05, **P < 0.01, ***P < 0.001; ns: no significant difference.

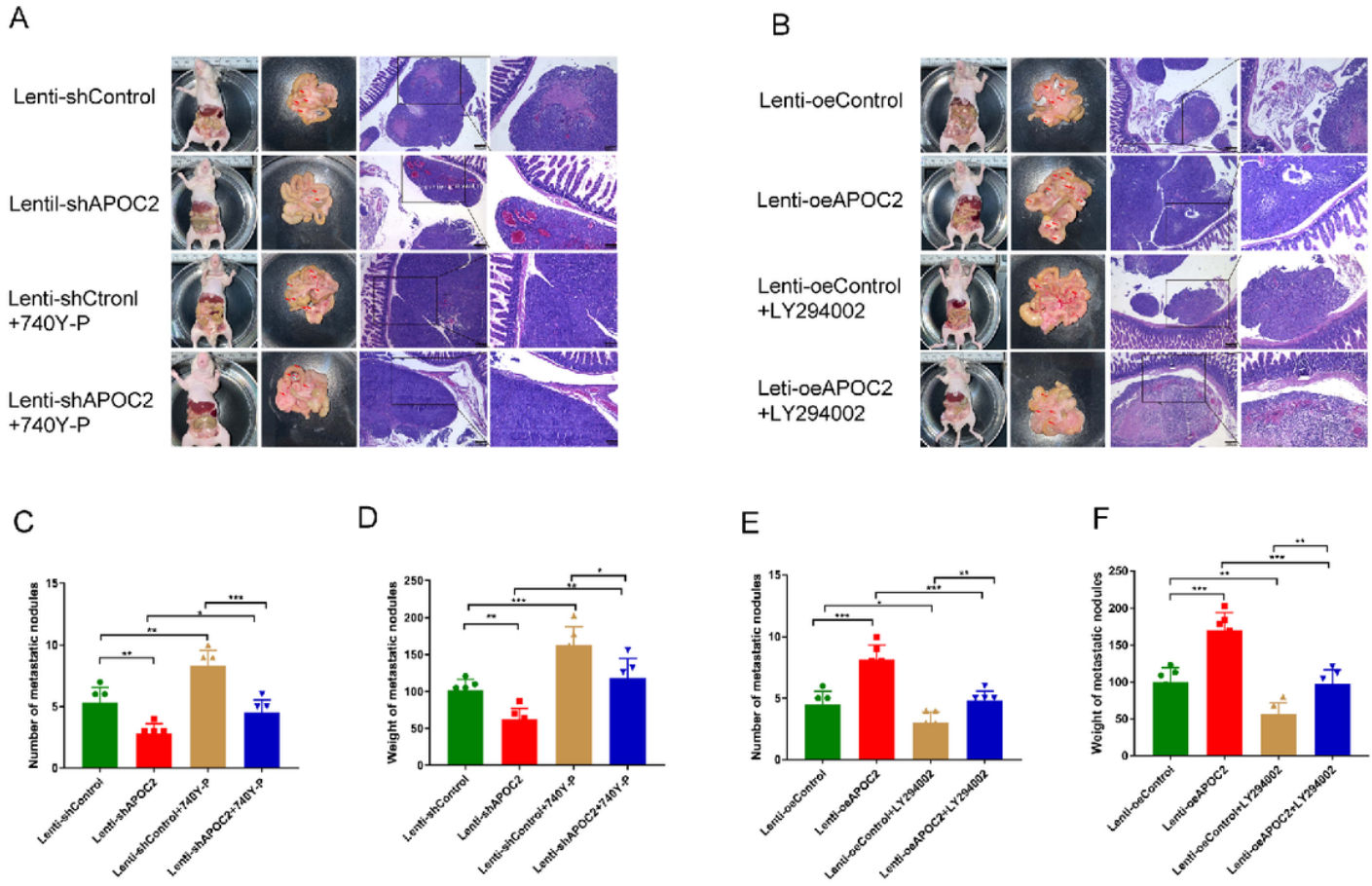

Figure 7

APOC2-mediated PM of GC cells in vivo. (A). Representative images of the macroscopic appearance and hematoxylin and eosin (H&E) staining of PM nodules in nude mice treated with the PI3K pathway activator by 740Y-P or intraperitoneal injection of AGS cells stably infected with Lenti-shControl or Lenti-shAPOC2 lentiviral particles (N = 6 per group). The total number (C) and weight (D) of PM nodules in the respective groups. (B) Representative images of the macroscopic appearance and H&E staining of PM nodules in nude mice treated with PI3K pathway inhibitor by LY294002 or intraperitoneal injection of AGS cells stably infected with Lenti-oeControl or Lenti-oeAPOC2 lentiviral particles (N = 6 per group). The total number (E) and weight (F) of PM nodules in the respective groups. Data represent mean ± SD. The level of significance is indicated by *P < 0.05, **P < 0.01, ***P < 0.001.

Supplementary Files

This is a list of supplementary files associated with this preprint. Click to download.

- Table1.xlsx
- TableS1metastasisVSprimary.xls
- TableS2metastasisVSprimaryUp.xls
- TableS3metastasisVSprimaryDown.xls
- TableS4Homosapiens.fa.GO2protein.xls
- TableS5metastasisVSprimary.GO2protein.xls
- TableS6Homosapiens.kog2protein.xls
- TableS7metastasisVSprimary.kog2protein.xls
- TableS8Homosapiens.KEGG2protein.xls
- TableS9metastasisVSprimary.KEGG2protein.xls
- TableS10metastasisVSprimary.protein2subcellular.xls
- TableS11metastasisVSprimary.network.relation.xls
- supplementFigure1.tif
- supplementary.docx